NASA Technical Memorandum 106639

Review of Slow-Wave Structures

Thomas M. Wallett and A. Haq Qureshi
Lewis Research Center
Cleveland, Ohio

June 1994

National Aeronautics and
Space Administration

REVIEW OF SLOW-WAVE STRUCTURES

Thomas Michael Wallett and A. Haq Qureshi*
National Aeronautics and Space Administration
Lewis Research Center
Cleveland, Ohio 44135

SUMMARY

The majority of recent theoretical and experimental reports published in the literature dealing with helical slow-wave structures focus on the dispersion characteristics and their effects due to the finite helix wire thickness and attenuation, dielectric loading, metal loading, and the introduction of plasma. In many papers, an effective dielectric constant is used to take into account helix wire dimensions and conductivity losses, while, the propagation constant of the signal and the interaction impedance of the structure are found to depend on the surface resistivity of the helix. Also, various dielectric supporting rods are simulated by one or several uniform cylinders having an effective dielectric constant, while metal vane loading and plasma effects are incorporated in the effective dielectric constant.

The papers dealing with coupled-cavities and folded or loaded wave guides describe equivalent circuit models, efficiency enhancement, and the prediction of instabilities for these structures. Equivalent circuit models of various structures are found using computer software programs SUPERFISH and TOUCHSTONE. Efficiency enhancement in tubes is achieved through dynamic velocity and phase adjusted tapers using computer techniques. The stability threshold of unwanted antisymmetric and higher order modes is predicted using SOS and MAGIC codes and the dependence of higher order modes on beam conductance, section length, and effective Q of a cavity is shown.

HELICAL STRUCTURES

Wire thickness and attenuation effects

A field analysis of a helix structure with a metal shield surrounded by a uniform cylindrical dielectric has been carried out by Tsutaki et al [1]. The design method for high performance helix traveling-wave tubes that evolved takes into account the effects of the helix tape width, dielectric permittivity, and shield barrel. The determination of the coefficients of the electric and magnetic field components involves the solution of a 6 × 6 matrix equation. There were however certain discrepancies in the resultant 6 × 6 matrix equation. Otsuka [2] showed that with a suitable choice of Bessel functions for the radial term of the z-components of the electric and magnetic fields, which vanish at the inner radius of the metal shield, the 6 × 6 matrix equation could be reduced to a 4 × 4 matrix equation. The corrected transmission loss is given as

$$L_s = (4.343/Z_0) \cdot [R_{s1}/(\pi\delta \sin \psi) + R_{s2}/(2\pi a_s)] \tag{1}$$

where δ is the diameter of the wire helix, a_s is the shield barrel radius, R_{s1} and R_{s2} are the surface resistances of the helix and shield barrel, respectively, Z_0 is the characteristic impedance, and ψ is the helix pitch angle. This is found to be valid for the cases where $\psi = 90°$ and $\psi = 0°$.

The theoretical dispersion characteristics of a helix with wire of finite thickness, supported by longitudinal dielectric rods of circular cross-section in a glass tube, were investigated by Jain et al [3]. An equivalent model of the structure was used for a field analysis using a cylindrically symmetric, homogeneous dielectric tube with an effective permittivity based on the support rod parameters (Figure 1).

---

*National Research Council—NASA Research Associate at Lewis Research Center.

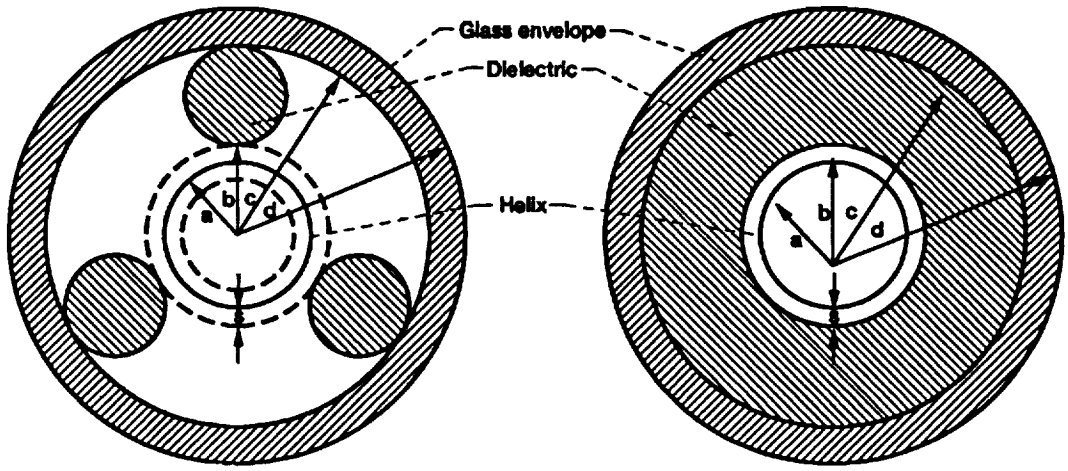

Figure 1 - (a) Cross section of the helix structure and (b) its equivalent model.

The relative volume occupied by the support rods in the structure is taken into account by the effective permittivity [4,5]. The effective permittivity is given as

$$\epsilon_{r,\ \mathrm{eff}} = 1 + (\epsilon_{r,\ \mathrm{rod}} - 1)\left(\frac{N}{4}\right)\left(\frac{d_{\mathrm{rod}}}{d_{\mathrm{rod}} + 2(a+s)}\right) \tag{2}$$

where $\epsilon_{r,\ \mathrm{rod}}$ is the relative permittivity of the support rods, d_{rod} is the rod diameter, and N is the number of rods. a and s are the mean helix radius and helix wire radius, respectively.

A dispersion relation was found as

$$(k/\gamma)\cot\psi = \left(\frac{\mathrm{I}_0(\gamma a)\ \mathrm{K}_0(\gamma a)}{\mathrm{I}_1(\gamma a)\ \mathrm{K}_1(\gamma a)}\right)^{1/2} \cdot D \simeq (v_p/v_c)\cot\psi. \tag{3}$$

In the above equation, k is the free space propagation constant, $\gamma = (\beta^2 - k^2)^{1/2}$ is the radial propagation constant, ψ is the helix pitch angle, v_p is the phase velocity, v_c is the speed of light, I_n and K_n are the nth order modified Bessel functions of the first and second kinds, respectively, and D is a dielectric loading factor.

The phase velocity as a function of frequency was experimentally determined for two representative structures, one at S band and the other at C band. Both structures are supported by three dielectric rods. Considering the finite wire thickness, it was found that the theoretically calculated values of phase velocity were in better agreement with the experimental results than the values calculated when the finite wire thickness was ignored. The interaction impedance of the C band structure was also calculated using standard methods and was shown to be

$$K = \left(\frac{1}{\xi v_p/v_c}\right)\cdot\eta \tag{4}$$

where η is the free space intrinsic impedance and ξ is a dimensionless parameter that depends on the structure geometry and material properties.

Properties of a helical slow-wave structure with dielectric supports, enclosed in a metal envelope, are affected not only by the relative volume, geometry, and permittivity of the supports, but also by the conductivity of the metal envelope. By ignoring losses due to the helix, envelope, and dielectric supports, a first order estimate of the properties can be found. Jain et al [6] have developed a theory of conductivity losses in a helix, having finite wire thickness, with dielectric supports, simulated by a cylindrically symmetric tube, in a metal envelope (Figure 2).

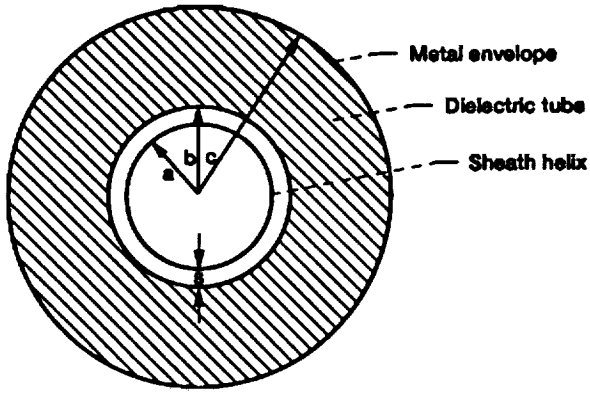

Figure 2 - Cross section of the equivalent helix structure to model conductivity losses.

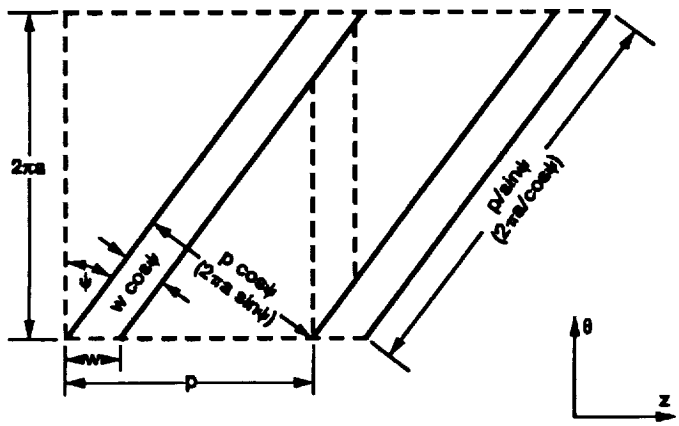

Figure 3 - The developed helix model with parameters for the equivalent helix structure.

The power loss per unit axial length for the helix and envelope was calculated through field analysis using both the sheath helix and tape helix models (Figure 3). The sum of these represented the total power loss per unit length. The total power flow through the structure was then calculated. Closed form expressions for the inductance per unit length L, capacitance per unit length C, and resistance per unit length R were derived along with other important parameters such as the attenuation constant α, axial phase constant β, and interaction impedance K. Calculations from 1 to 15 GHz revealed that when the relative permittivity of the supports increased, C increased, but L and R decreased. The effects were more noticeable for L and C at higher frequencies and for R at intermediate frequencies. Also L decreased, C increased, and R initially decreased then increased as the envelope radius c was reduced. The effects were again more noticeable for R at intermediate frequencies, however, for L and C they were more prominent at lower frequencies.

The attenuation constant α and the phase constant β were found to increase in magnitude with higher frequency, greater support permittivity, and smaller envelope radius. At higher frequencies, the change in support permittivity had a greater effect on them than the change in envelope radius.

The interaction impedance K, however, was found to decrease with respect to these changes, especially at lower frequencies. For less than a tenfold increase in the helix and envelope resistivities there is virtually no change in β and K; however, α and R increase considerably, especially at high frequencies.

The normalized attenuation constant as a function of normalized frequency γa was determined using c/a as a parameter and compared with the results of Rowe [7] for a helix in free space. The normalized attenuation constant was also determined using cot ψ and s as parameters and compared with the results of Bryant and White [8]. It appeared that α increased as c/a decreased or as cot ψ increased and s decreased.

Using the tape model for the helix, the attenuation constant was determined as a function of frequency and compared to the experimental and theoretical sheath model results of Gilmour et al [9]. The tape model showed considerably better agreement with the experimental values than their own sheath model.

The effects of having an attenuator-coated helical slow-wave structure were considered by Jain and Basu [10]. Two structures were theoretically analyzed. Both structures contained a helix inside a dielectric tube with an outer metal envelope (Figure 4).

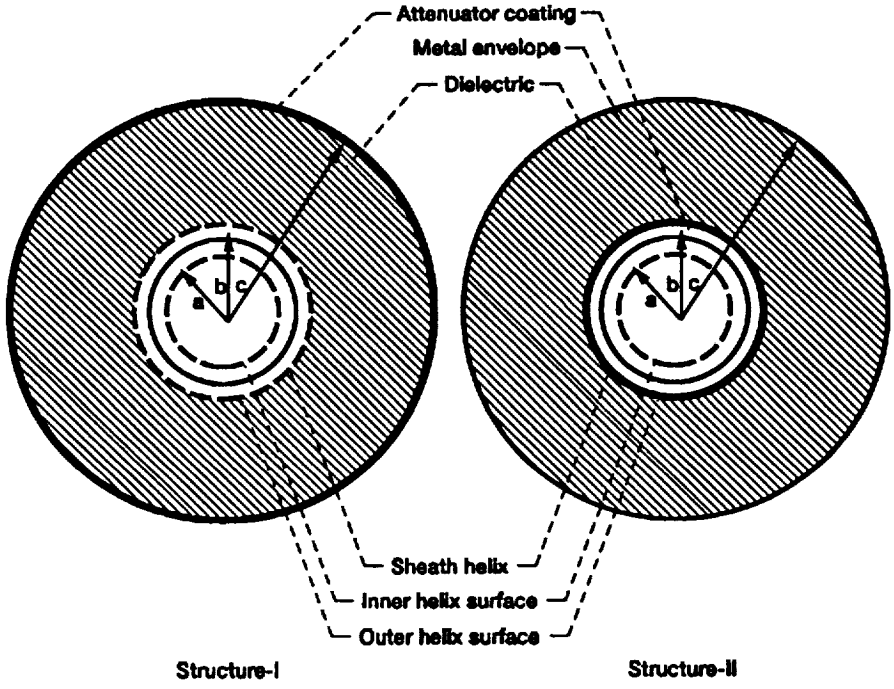

Figure 4 - Helical slow-wave structures with an attenuator coating (Structure I) on the outer surface of a dielectric tube and (Structure II) on the inner surface of a dielectric tube.

A resistive coating was placed on the outside of the dielectric tube in structure I while structure II had a resistive coating on the inside of the dielectric tube. The sheath helix model was used and helix thickness was taken into account. The field expressions with the appropriate boundary conditions lead to the following dispersion relations for the two structures:

$$\frac{k^2 \cot^2\psi}{\gamma^2} = \frac{I_0(\gamma a)\cdot(K_0(\gamma a) + M I_0(\gamma a))}{I_1(\gamma a)\cdot(K_1(\gamma a) - N I_1(\gamma a))} \quad \text{(structure I)} \tag{5}$$

$$\frac{k^2 \cot^2\psi}{\gamma^2} = \frac{I_0(\gamma a)\cdot(K_0(\gamma a) + PI_0(\gamma a))}{I_1(\gamma a)\cdot(K_1(\gamma a) - QI_1(\gamma a))} \quad \text{(structure II)}. \tag{6}$$

The parameters M, N, P, and Q depend on the frequency, structure, and material properties.

The dependence of the attenuation constant α, phase constant β, and interaction impedance K, on surface resistivity R_s, for various frequencies between 2 and 10 GHz in 2 GHz increments was evaluated.

It was found that in both structures α increases sharply, reaching a peak, and then appears to exponentially decrease as R_s increases, with their values being greater and peaks being sharper in structure II than in structure I.

In structure I, β decreases below a certain frequency, while above a higher frequency β tends to increase, as R_s is increased. In structure II, β increases as R_s increases, especially at lower values of R_s.

The interaction impedance K, generally increases as R_s increases in structure I, however, in structure II, above a certain frequency, K will pass through a maximum as R_s is increased.

The dependence of α, β, and K with frequency was also investigated using the metal envelope radius per sheath helix radius c/a, R_s, ϵ_r, and cot ψ as parameters. The values used for c/a ranged from 1.25 to 3.00. In both structures, α increases with increasing frequency and exhibits sharper maxima at specific values of R_s. Also, the value of R_s where a maximum occurs increases with f in both structures followed by a drop with f only in structure I.

In general, α increases to a maximum and then decreases slowly as f increases for structure I for a given c/a. The maximum for α and the corresponding frequency increase as c/a becomes smaller. This corresponding frequency can also be increased by increasing R_s, decreasing ϵ_r, or decreasing cot ψ. For structure II, there is a steady increase in α as frequency increases with the values of α being larger for larger c/a. The attenuation is also affected by cot ψ, and ϵ_r at midrange frequencies.

The phase constant β increases as frequency increases for both structures. The increase in β is larger for lower R_s in structure I and smaller for higher R_s in structure II. However, in structure I, at very high frequencies, β is essentially independent of the effects of the attenuator coating.

The frequency response of β is more sensitive for both structures at lower R_s, particularly for structure II. The frequency response becomes sensitive in structure I as c/a is increased and in structure II as c/a is decreased, especially at very low values. The frequency response is, also, quite sensitive to ϵ_r in both structures.

As for the interaction impedance, the higher the frequency, the lower the values of K in both structures. The interaction impedance K can be increased by decreasing c/a for structure I or increasing c/a for structure II.

The frequency response sensitivity of K was more pronounced at lower values of R_s for both structures while at lower frequencies for structure I and higher frequencies for structure II. It was also found that the normalized phase velocity decreased while the small-signal gain increased in structure II as the attenuator coating R_s increased over the frequency range of 1 to 15 GHz.

These results were compared with the work of Webber [11] and Caldwell [12] and although the results qualitatively explained their work, quantitative results could not be verified due to lack of pertinent data.

Dielectric loading, metal loading, and plasma effects

Helical slow-wave structures supported by dielectric rods of circular cross section and rectangular cross section enclosed in metal envelopes were theoretically analyzed by Jain and Basu [13] using two approaches (Figure 5).

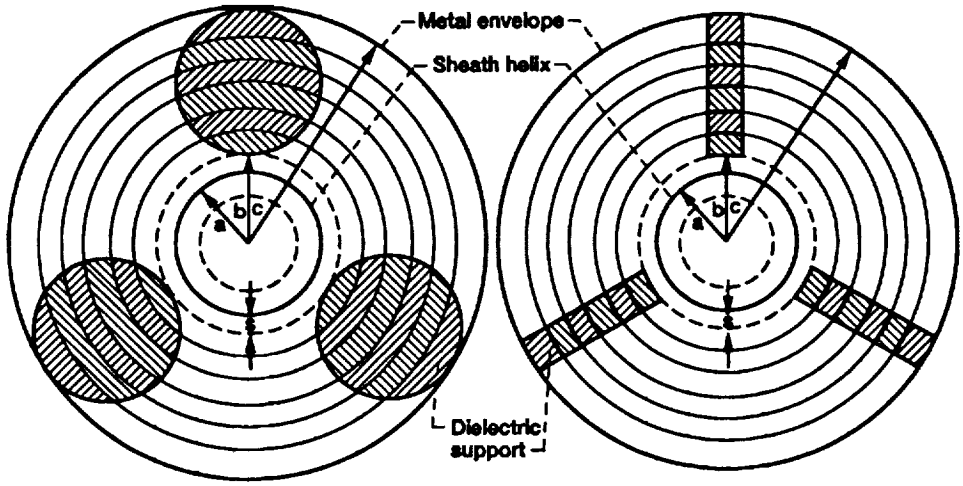

Figure 5 - Helical structures with circular dielectric rods and rectangular dielectric bars.

In the first approach, the support rods are replaced by a single homogeneous coaxial dielectric tube with an effective permittivity, taking into account the relative volume occupied by the rods. The second approach is to use several homogeneous coaxial dielectric tubes each with an effective permittivity determined from the amount of dielectric material contained in the volume occupied by the particular tube. The effective permittivities using both approaches also were calculated taking into account the finite helix thickness. The subsequent dispersion relations were determined for both types of support rods choosing a metal envelope radius to mean helix radius c/a of 1.4 and varying the support dielectric permittivity by choosing quartz ($\epsilon_r = 3.8$), anisotropic pyrolytic boron nitride APBN ($\epsilon_r = 5.1$), and alumina ($\epsilon_r = 9.0$). The dispersion relations for alumina support rods were also obtained using values of 1.2, 1.6, 2.0, and 2.4 for c/a.

In general, the dispersion values using the second approach were slightly higher than those using the first approach, in the case of circular supports; however, they were slightly lower in the case of rectangular supports. The normalized phase velocities calculated for frequencies between 2 and 14 GHz using both approaches were compared to the experimental results of Putz and Cascone [14] for the structure with supports having rectangular cross-section and those of Belohoubek [15] for the structure with supports of circular cross-section. In both cases, the second approach was in better agreement with the experimental results.

There was a considerable disparity between the two approaches when
1) the frequency was increased,
2) the separation between the metal envelope and helix was increased, or
3) dielectric rods of higher relative permittivity were used.

Another analysis of dispersion characteristics for an inhomogeneously loaded helical slow-wave structure supported by unconventional types of dielectric rods in a metal envelope is given by Kapoor et al [16]. The method of approach here was to divide the volume into concentric tubes and calculate an effective dielectric constant for each tube based on the portion of the dielectric material in that tube.

The effective dielectric constant of the pth tube, with $1 \leq p \leq n$, is given by

$$\epsilon_{rp} = 1 + N(\epsilon_r - 1)A_{sp}/A_p \tag{7}$$

where N is the number of support rods, ϵ_r is the relative permittivity of the rods, and n is the number of concentric dielectric tubes. A_{sp} is the cross-sectional area of the part of the dielectric rod in the pth tube and A_p is the cross-sectional area of the pth tube.

A general form for the dispersion relation of a helix structure with unconventional supports is found in terms of a dielectric loading factor. The dispersion relation is

$$\frac{v_p \cot \psi}{v_c} = \frac{k \cot \psi}{\gamma} = \left[\frac{I_0(\gamma a)K_0(\gamma a)}{I_0(\gamma a)K_0(\gamma a)}\right]^{1/2} \cdot D \tag{8}$$

where D represents the dielectric loading factor which depends on the effective dielectric constants for the particular dielectric supports.

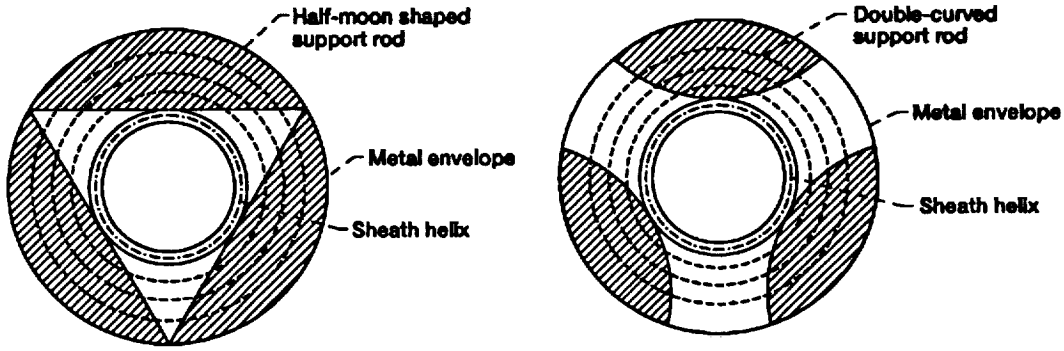

Figure 6 - Helical structures with half-moon and double-curved dielectric support rods.

Two types of dielectric supports, the half-moon shaped and double-curved rods, were considered for analysis (Figure 6). Theoretical values of the normalized phase velocity v_p/v_c for frequencies ranging from 1 to 15 GHz were calculated for the half-moon shaped rod and the double-curved rod structures. The calculations were performed using $n = 12$ for the number of tubes. The inner and outer helix diameters for both structures were 0.06 in. and 0.07 in., respectively, and the radius of curvature for the side adjacent to the helix in the double-curved rod structure was 0.075 inches.

The dispersion characteristics of both structures were compared to the experimental results of Belohoubek [15] and found to agree within 5 to 9 per cent over the entire frequency range. Furthermore, the v_p/v_c values calculated with $n \geq 12$ were within 0.2 per cent of the experimentally measured values and the agreement further improves as n becomes larger.

The effect of varying the permittivity on the dispersion characteristics for the half-moon structure was investigated for the metal envelope to mean helix radii ratio of $c/a = 1.8$. The values of ϵ_r chosen were 5.1 (APBN), 6.6 (Beryllia), and 9.0 (Alumina). As ϵ_r increased, the phase velocity decreased and a more negative dispersion resulted. Likewise, varying c/a from 1.2 to 2.0 in increments of 0.2, with $a = 0.08255$ cm. and $\epsilon_r = 9.0$, resulted in lower phase velocities and also a higher negative dispersion.

Calculated values of the interaction impedance for both structures showed a slightly higher impedance for the double-curved rod structure than the half-moon shaped rod structure across the frequency range.

An empirical method of calculating the interaction impedance of dielectric-loaded helix structures was formulated by Singh [17] et al. Two structures, with and without metal envelopes, were considered having the ratio of envelope to helix radii of two to one ($c/a = 2.00$) with a homogeneous, cylindrically symmetric, dielectric tube of permittivity $\epsilon_r = 1.41$ located between the envelope and the helix. The homogeneous dielectric can in fact be simulated by several long dielectric rod supports.

A theoretical field analysis was made to calculate the power flow through both dielectric-loaded structures leading to the following expression for the interaction impedance

$$K = \frac{(\gamma/\beta)^4}{\pi(k/\beta)F}\left(\frac{\mu_0}{\epsilon_0}\right)^{1/2} \tag{9}$$

where k, γ, and β represent the free space, radial, and axial propagation constants, respectively, and F is a structure parameter.

The characteristic impedance of the structures was also shown to be of the form

$$Z = Z_0\left(\frac{\alpha_L}{\alpha_C}\right)^{1/2} \tag{10}$$

where the characteristic impedance Z_0 of the unloaded, free space helix is calculated by standard methods [18] while α_L and α_C are the normalized inductance and capacitance per unit length of the structure with respect to the unloaded, free space helix.

Similarly, an empirical formula for the interaction impedance was chosen as

$$K = K_0\left[\left(\frac{\alpha_L}{\alpha_C}\right)^{1/2}\right]^{m/n} \tag{11}$$

with K_0 being the interaction impedance of the unloaded, free space helix.

The empirical formula, Equation (11), was found to agree very well with the theoretical values using Equation (9) when $m = 4$ and $n = 3$ for the structure with the metal envelope and when $m = 2$ and $n = 3$ for the structure without the metal envelope. The formula also works fairly well for other values of c/a and ϵ_r. Thus, by knowing the unloaded, free space parameters for the helix and the circuit parameters of the loaded structure, one can estimate the interaction impedance of the loaded structure.

The dispersion characteristics for a traveling-wave tube consisting of a helix in a metallic cylindrical wave guide are altered to a great extent when the helix is supported by dielectric material or by the introduction of plasma into the wave guide. Mishra et al [19] have determined the dispersion relations of the fundamental azimuthally symmetric mode for the helix wave guide with and without dielectric supports and the plasma-filled helix wave guide.

A tape helix with zero thickness was considered for the model. The pitch angle ψ of the helix is defined by $\cot \psi = 2\pi a/L$ where L is the period and a is the radius of the helix. Appropriate boundary conditions were then applied to solve for the dispersion relations [20,21,22].

The model of the structure used for analysis has a tubular dielectric support of thickness $c - a$, where c is the outer radius of the dielectric cylinder or metallic envelope radius and a is the inner radius or helix radius (Figure 7).

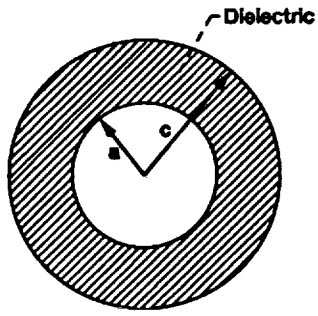

Figure 7 - Helix structure with a dielectric support having an inner radius a and outer radius c.

The dispersion relation is

$$\frac{(a^2\omega^2/v_c^{\,2})\cot^2\psi}{(a^2\beta_0^{\,2}-a^2\omega^2/v_c^{\,2})}=\frac{\mathrm{J}_0^{\,2}(pa)}{\mathrm{J}_1^{\,2}(pa)}\frac{1-q/p\cdot F'(a,\,c)}{1-\epsilon p/q\cdot F(a,\,c)}. \tag{12}$$

Here,

$$F(a,c)=\frac{\mathrm{J}_0(pa)}{\mathrm{J}_1(pa)}\cdot\frac{\mathrm{J}_1(qa)\mathrm{Y}_0(qc)-\mathrm{J}_0(qc)\mathrm{Y}_1(qa)}{\mathrm{J}_0(qa)\mathrm{Y}_0(qc)-\mathrm{J}_0(qc)\mathrm{Y}_0(qa)} \tag{13}$$

and

$$F'(a,c)=\frac{\mathrm{J}_1(pa)}{\mathrm{J}_0(pa)}\cdot\frac{\mathrm{J}_0(qa)\mathrm{Y}_1(qc)-\mathrm{J}_1(qc)\mathrm{Y}_0(qa)}{\mathrm{J}_1(qa)\mathrm{Y}_1(qc)-\mathrm{J}_1(qc)\mathrm{Y}_1(qa)} \tag{14}$$

with $p^2=(\omega^2/v_c^{\,2}-\beta_0^{\,2})$ and $q^2=(\omega^2\epsilon/v_c^{\,2}-\beta_0^{\,2})$. J_n and Y_n are nth order Bessel functions of the first and second kind, respectively.

When the dielectric support is replaced by vacuum, the dispersion relation becomes

$$\frac{(a^2\omega^2/v_c^{\,2})\cot^2\psi}{(a^2\beta_0^{\,2}-a^2\omega^2/v_c^{\,2})}=\frac{\mathrm{J}_0(pa)\mathrm{J}_1(pc)}{\mathrm{J}_0(pc)\mathrm{J}_1(pa)}\cdot\frac{\mathrm{J}_0(pc)\mathrm{Y}_0(pa)-\mathrm{J}_0(pa)\mathrm{Y}_0(pc)}{\mathrm{J}_1(pa)\mathrm{Y}_1(pc)-\mathrm{J}_1(pc)\mathrm{Y}_1(pa)}. \tag{15}$$

As c approaches a, the dispersion relation exhibits three distinct modes: a TE-like, TM-like, and helix mode. The helix mode satisfies $a\omega/v_c=a\beta_0\sin\psi$.

Considering the dispersion relation for a plasma-filled helix wave guide without dielectric supports yields

$$\frac{(a^2\omega^2/v_c^{\,2})\cot^2\psi}{(a^2\beta_0^{\,2}-a^2\omega^2/v_c^{\,2})}=\frac{\mathrm{J}_0(ka)\mathrm{J}_1(kc)}{\mathrm{J}_0(kc)\mathrm{J}_1(ka)}\cdot\frac{\mathrm{J}_0(ka)\mathrm{Y}_0(kc)-\mathrm{J}_0(kc)\mathrm{Y}_0(ka)}{\mathrm{J}_1(ka)\mathrm{Y}_1(kc)-\mathrm{J}_1(kc)\mathrm{Y}_1(ka)}. \tag{16}$$

In the limit as c approaches a and for $\omega_P^{\,2}/\omega^2\ll 1$, the helix mode satisfies the relationship

$$a^2\omega^2/v_c^{\,2}=a^2\beta_0^{\,2}\sin^2\psi+(a^2\omega_P^{\,2}/v_c^{\,2})\cos^2\psi. \tag{17}$$

Results for the helix wave guide with dielectric supports were numerically determined for two sets of parameters: $c/a=1.5$, $\epsilon=4.0$, $\psi=30^\circ$, 40°, 50°, 60° and $\psi=30^\circ$, $\epsilon=4.0$, $c/a=1.5$, 1.8, 2.0.

From the resulting dispersion relations for these sets of data, several points are noted.

1) Restricted electromagnetic wave propagation exists in the region $\beta_0^2 v_c^2/\epsilon < \omega^2 < \beta_0^2 v_c^2$ in the presence of the dielectric.
2) The helix mode for the helix wave guide without dielectric supports does not properly describe the shape of the dispersion curve, especially at large c/a [22]. The addition of the dielectric supports tends to simply flatten the curves.
3) For the helix wave guide with dielectric supports, the phase velocity of the modes is roughly proportional to the frequency and inversely proportional to c/a and ψ. Also, for large β_0, the group velocity approaches $v_c/\sqrt{\epsilon}$.

The helix modes were determined for a plasma-filled helix wave guide using the parameters $\psi = 30^\circ$ and $a^2\omega_P^2/v_c^2 = 0.0$, 0.4, and 0.8. The effect of the plasma is to increase the low frequency cutoff. Higher beam currents and shorter wavelengths can be generated for the same beam power. The device performance can be optimized with the proper choice of geometry, dielectric material, and plasma density.

In high power traveling-wave tubes the possibility of backward wave oscillations is reduced by using a contrawound helix (Figure 8a) or ring bar structure (Figure 8b) instead of a single helix.

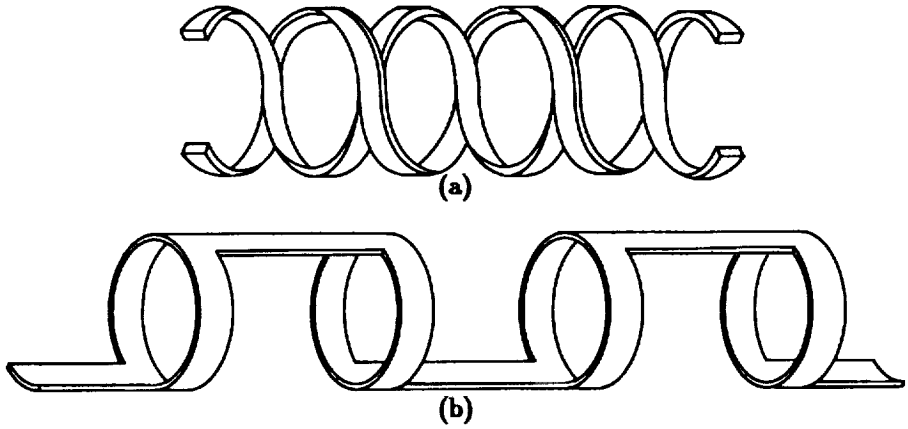

Figure 8 - (a) The two tape contrawound helix and (b) its ring-bar version.

The effect of dielectric and metal loading on the dispersion characteristics of contrawound helices was investigated by Cain and Grow [23]. They considered the theoretical dispersion characteristics of an infinitesimally thin contrawound helix between two dielectric regions of different permittivity. As the permittivity of the outer dielectric is increased from 1 to 9 with respect to the inner dielectric, the phase velocity and group velocity decrease. The same result was also shown to be true for a single helix. This result had been experimentally determined previously by Birdsall and Everhart [24].

The dispersion characteristics of a contrawound helix with finite thickness, surrounded by a dielectric tube, were experimentally determined and found to exhibit lower phase and group velocities, except for low β, compared to the theoretically determined characteristics of the thin helix. While maintaining the same outer tube diameter, it was also noticed that phase velocity decreased as the distance between the helix and the inner dielectric tube was reduced. Past a certain distance, however, dielectric loading was negligible.

The effect of varying the helix pitch angle on the theoretical dispersion characteristics for a contrawound helix between two dielectric media was investigated for the cases when the ratio of permittivities of the outer to inner dielectric was 1.5 and 9. In both cases the phase velocity and group velocity decreased as the cotangent of the pitch angle increased.

The theoretically calculated values of the dispersion characteristics are strongly influenced by the degree of metal loading with an outer conducting cylinder. Regions in the dispersion characteristics associated with the open structures of the dielectric-loaded helix where a wave is not supported disappear when an outer conducting cylinder is added.

For the case of dielectric and metal loading, the net effect is simply the superposition of the individual effects due to each. In general, the phase and group velocities are decreased whenever dielectric material is added. Also, as metal loading is increased, dispersion is reduced.

Dispersion shaping can be accomplished by loading a slow-wave structure with metal vanes. Metal-vane-loaded helical slow-wave structures with many thin vanes can be analyzed using a technique which considers an infinite number of vanes (INV) of infinitesimal thickness [25,26,27] with the entire structure enclosed in a metal envelope.

In this technique the vanes are assumed to affect only the axial electric field and not the azimuthal electric field. A rigorous theoretical analysis was given by Kravchenko et al [28] to predict dispersion in structures with a certain number of vanes having specific angular thicknesses. By considering this analysis and various experimental data [14,29,30,31], it was found that a smaller than actual vane tip to helix separation is needed for the INV technique to correctly predict the dispersion for a vane-loaded structure with relatively few vanes.

In the INV technique, two models of the structure are used for the solution of the fields: one for the axial component and one for the azimuthal component (Figure 9).

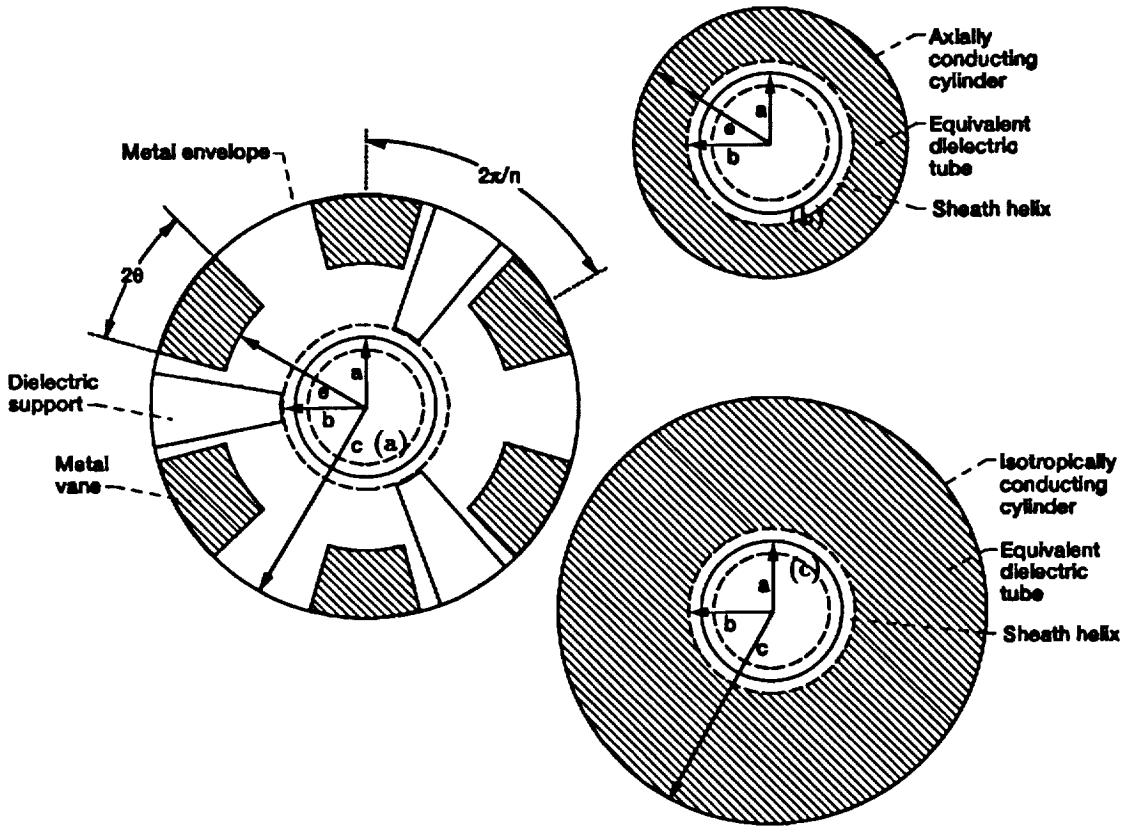

Figure 9 - (a) Cross sectional geometry of the vane-loaded slow-wave structure, (b) the model used for the axial field component, and (c) the model used for the azimuthal component.

Both models are divided into three regions. The three distinct regions are:
1) the region inside the mean helix radius a,
2) the region from the mean helix radius a to outer helix radius b, and
3) an outer equivalent dielectric region enclosed by a conducting cylinder.

In the model for the axial field solution, the outer dielectric region extends only to the tips of the vanes where it is enclosed in a metal cylinder of radius e conducting only in the axial direction, whereas in the azimuthal model, the outer dielectric region extends to the actual metal envelope of radius c.

A modified version of the INV technique (MINV) was developed by Kumar et al [32] to take into account the finite number n and angular thickness θ of the vanes for practical structures. The inter-vane axial electric field is found from [33] with which the amount of penetration into the vanes can be deduced. A new value of the axially conducting cylinder radius e can then be found for use in the INV technique.

The dispersion characteristics were found using the MINV technique for a vane-loaded structure with $n = 6$, $\theta = \pi/24$, $\epsilon_r = 1.0$, and $b/a = 1.0$ while $e/a = 1.2$ with $c/e = 1.2$, 1.4, 2.6 and $e/a = 1.4$ with $c/e = 1.0$, 1.2, 1.8, 2.6. The results compared well with those obtained using the field analysis of Kravchenko [33] when the value for e is such that the axial electric field strength there is 55% of the value at the vane tips. Upon further comparison for $c/a = 2.52$ and $e/a = 1.4$, the MINV technique was within 2% of Kravchenko's results while the INV technique was only within 14%.

The INV technique still remains useful, however, in adequately predicting the dispersion characteristics of structures with large numbers of thin vanes. Close agreement was found between experimental results of Scott [29] and theoretical values employing the INV technique on a structure using three boron nitride supports for the helix structure and three quartz segments with 39 photoetched metallic lines for vanes.

The dispersion characteristics calculated by both the MINV technique and the INV technique were compared to the experimental results of Galuppi and Salvatore [31] for a structure with $n = 3$ vanes, $\theta = \pi/6$, $c/a = 2.11$, and $b/a = 1.05$ and two sets of parameters: $e/a = 1.68$ with $\epsilon_{r,\,eff} = 2.19$ and $e/a = 1.26$ with $\epsilon_{r,\,eff} = 2.14$. The MINV technique was much closer in agreement than the INV technique. Also, the characteristic and interaction impedances using the MINV theory were higher than those calculated using the INV model for a structure with $a = 1.9$ mm, 2.1 mm pitch, $e/a = 1.5$, $c/a = 2.1$, $n = 3$, $\theta = 30°$, and $\epsilon_{r,\,eff} = 2.14$.

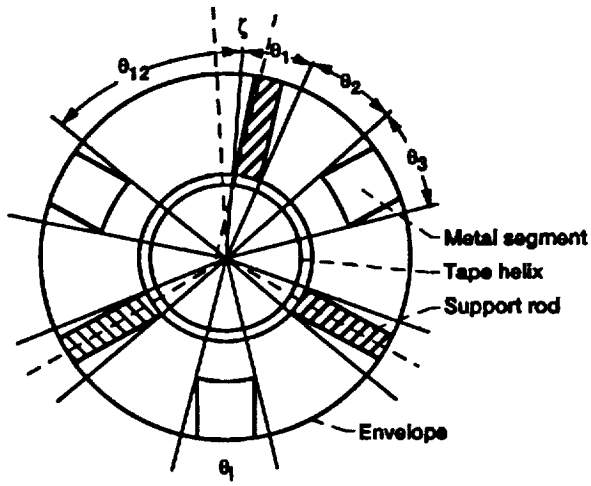

Figure 10 - Cross section of a solid-segment-loaded helix structure.

Metal-segment-loaded helices can be used for phase velocity dispersion shaping (Figure 10). Onodera and Raub [34] have developed an accurate formula for predicting the phase velocity dispersion of tape helices supported by dielectric rods with solid or vane type metal-segment-loading. The helix circuit is analyzed as a developed tape helix loaded with generalized metal segments (Figure 11).

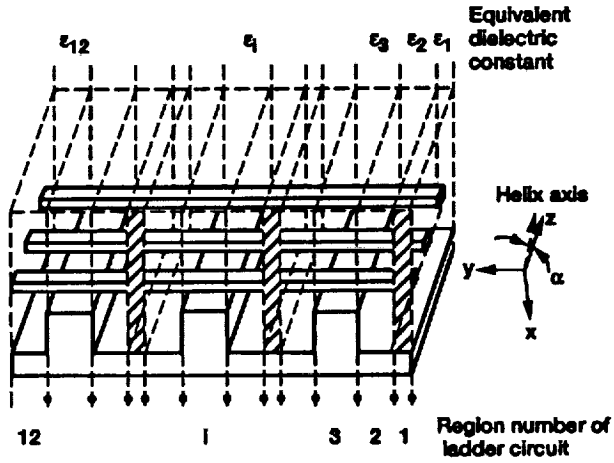

Figure 11 - Analytical model of the solid-segment-loaded helix structure.

An effective sheath helix radius is determined from a tape helix with finite thickness and an equivalent dielectric constant is then found for each section. If β and γ are propagation constants along the helix axis and z-axis, respectively, then $\gamma = \beta \cos \alpha$. When analyzed as i cascaded sections, the transmission matrix of the ith section in the y-direction is shown to be

$$M_i = \begin{bmatrix} \cos(\kappa_i l_i) & -jZ_i \sin(\kappa_i l_i) \\ -j\dfrac{\sin(\kappa_i l_i)}{Z_i} & \cos(\kappa_i l_i) \end{bmatrix} \tag{18}$$

where $\kappa_i = \sqrt{\epsilon_i}\,\kappa$ and $Z_i = Z_{0i}/\sqrt{\epsilon_i}$. κ_i and κ are the propagation constants along the y-axis of the ith section in the equivalent dielectric ϵ_i and in free space, respectively. l_i is the arc length of the ith loading element at mean radius. Z_i and Z_{0i} are the characteristic impedances of the ith section in ϵ_i and in free space, respectively.

The total transmission matrix is given as

$$\left(M_{(2m+2)} \cdot M_{(2m+1)} \cdot \cdots \cdot M_2 \cdot M_1\right)^n = \begin{bmatrix} A & B \\ C & D \end{bmatrix} \tag{19}$$

where m is the segment number in the loading set number n. The relationship $AD - BC = 1$ holds.

The improved accuracy over other methods [14,25,35] is due to considerations of the helix thickness and edge effects of the metal segments. The edge effect of a metal segment is incorporated in a stray capacitance given by $C_s = C_d \cdot w_t \cdot M_c \cdot R$ where $C_d = 0.2\ \epsilon_0$, w_t is the width of the tape helix, M_c is a correction factor due to wave propagation effects, and R is a reduction factor due to dielectric loading and vane loading.

Since there are edge effects on both sides of the segments each M_i matrix must then be replaced by $N \cdot M_i \cdot N$, where

$$N = \begin{bmatrix} 1 & 0 \\ j\omega C_s & 1 \end{bmatrix}. \tag{20}$$

Each M_i matrix must be considered separately when asymmetries occur among different sets of loading elements.

Four solid and one vane type metal-segment-loaded helix circuits were built. The experimental phase velocity was measured over a normalized frequency range from 1.0 to 3.0 [35]. Calculations of the phase velocity for the solid-type and vane-type circuits were compared to the experimental results and estimated to be within $\pm 1\%$.

For $\gamma a < 0.75$ the formula predicts values for phase velocities that are too low. This may be due to inaccuracies in the calculation of the equivalent dielectric constant. In general, however, a metal segment or dielectric rod can be offset as much as $\pm 10^\circ$ from the normal position without an appreciable effect on the phase velocity. There is not much effect even when several segments or rods are rotated relative to each other as much as $\pm 10^\circ$. Also, the change in phase velocity due to a change in the dimensions of a loading element in a set is about 1/3 the change due to similar changes in the dimensions of three elements in three different sets.

Various asymmetries can affect the frequency where the π-mode stopband exists in a metal-segment-loaded helix circuit. Onodera [36] has considered some possible asymmetries as:
1) Angular offset of the support rod,
2) Variation of the support rod permittivity,
3) Variation of the support rod width,
4) Angular offset of the metal segment,
5) Variation of the helix/metal segment gap, and
6) Variation of the metal segment width.

The first two of these asymmetries were considered by Lien [37] using coupled-mode theory to analyze the stopband. Onodera points out that only the relative frequency and not the absolute frequency of the stopband can be calculated by Lien. Also, metal segments are not considered in his model.

By using an analytical model and the method of Onodera and Raub [34] for vane loading, a transfer matrix for one complete turn is found from the transfer matrices of each ladder circuit. The form of the matrix is given as

$$T = M_1 \cdot M_2 \cdots M_i \cdots M_{12} = \begin{bmatrix} A & B \\ C & D \end{bmatrix} \tag{21}$$

where M_i represents the transfer matrix for the ith ladder circuit.

Using Floquet's theorem, the relationship

$$e^{-\zeta\phi} = \frac{A+D}{2} - \sqrt{\left(\frac{A+D}{2}\right)^2 - 1}, \tag{22}$$

is found where ϕ represents the phase shift per turn and ζ is the offset angle of the support rod. The phase shift per turn is determined for the case $|(A+D)/2| < 1$ and the attenuation per turn is obtained for the case $|(A+D)/2| > 1$.

The calculated value (7.90 GHz) for the π-mode frequency for a solid metal-segment-loaded helix was within $\pm 1\%$ of the experimental value (7.96 GHz). The calculation of the attenuation constant as a function of offset angle also compares very well with the results of Lien [37]. It was found that the maximum attenuation varies exponentially with the width of the gap between the inner metal segment radius and the outer tape helix radius and linearly with the change in the support rod offset angle.

The small signal gain of a general broad-band helix TWT was calculated by Onodera [38] using two methods, the standard method established by Pierce [18] and a revised method using a finite beam thickness suggested by Ura [39,40] (Figure 12).

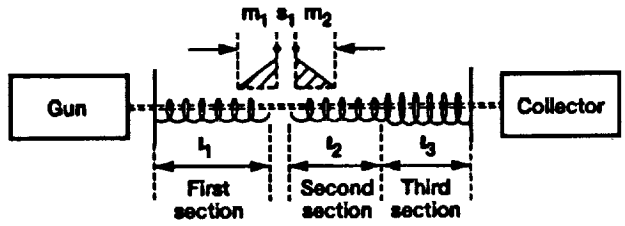

Figure 12 - Conceptual view of a multisectioned helix-type traveling-wave tube.

The equations for the gain parameter, C, and the space charge parameter, QC, are different in the two methods. In the Pierce theory, the average coupling impedance over the beam cross section is calculated as

$$K = \overline{K} = Z_{axis} \cdot \frac{\int_0^{r_0} I_0^2(\gamma_1 r) \cdot r \, dr}{r_0^2/2}. \tag{23}$$

Here, $\overline{K}$ is the average coupling impedance over the beam cross section without the beam, Z_{axis} is the coupling impedance on the axis of the helix without the beam, γ_1 is the radial propagation constant, and r_0 is the beam radius. C is then calculated as

$$C^3 = \frac{I_0 K}{4V_0'} \tag{24}$$

where I_0 is the beam current and V_0' is the effective beam voltage after correction for potential depression. Considering the plasma reduction factor F, the space charge parameter is given as

$$QC = \frac{1}{4C^2} \cdot \left(\frac{\omega_q/\omega}{1 + \omega_q/\omega} \right)^2 \tag{25}$$

where $\omega_q/\omega = F \cdot \omega_p/\omega$.

The average coupling impedance K and the space charge factor QC according to the Ura theory are given as

$$K = \overline{K} \cdot \frac{K}{\overline{K}} \tag{26}$$

and

$$QC = \frac{1}{4C^2} \cdot \frac{I_0}{V_0'} \cdot (Q_1 K - Q_2 K - Q_3 K). \tag{27}$$

In the previous expression Q_1K represents the space-charge field without a traveling-wave circuit, Q_2K represents the perturbed space-charge field due to the beam independent of the circuit, and Q_3K represents the perturbed space-charge field due to the beam dependent on the circuit. Q_3K is approximated by that of an ideal sheath helix.

Three broad-band helical TWTs were then built and tested. The small signal gain was experimentally determined and theoretically calculated using both methods for each TWT. The calculations performed were based on the following parameters.

1) The beam radius used contained 95% of the beam based on trajectory analysis.
2) The beam voltage and current used were the experimental values of the tubes.
3) The helix circuit characteristics were based on cold test measurements.
4) The active helix lengths for the first and second sections were taken as the lengths of the distributed loss less half the terminated loss of the appropriate section. The active length of the third section was simply the length of the distributed loss of that section.
5) The sever length was taken as half the sum of the terminated loss lengths of the first two sections plus the length of the drift space between the first two sections.
6) The sever loss of the first section was approximated at -6 dB while the sever losses of the second and third sections were taken to be zero.

Values of QC also were calculated for all three TWTs using the standard method, with and without an infinite drift tube radius, and the Ura method. From the calculations and experimental data, the following conclusions were drawn.

1) The small signal gain calculated by the improved method was in better agreement with experimental values over a normalized frequency range with respect to the cutoff from 1.0 to 2.0 than the standard method. In particular, there was very good agreement for the maximum gain and frequency at maximum gain.
2) The values of QC calculated using this method were higher than those calculated from plasma reduction factors based on a drift tube with infinite radius.
3) The gain in the terminated loss region of the TWTs can be approximated by assuming the active length of the first section, including terminated loss, is increased by one half of the length of the terminated loss.

COUPLED-CAVITY AND PERIODIC WAVE GUIDE STRUCTURES

Circuit models

Rippled-wall cylindrical wave guide structures have applications in the area of high power microwave devices. Kantrowitz and Adler [41] have used a transmission line equivalent circuit model to describe these structures in order to calculate the dispersion relations for the TM_{0n} modes (Figure 13).

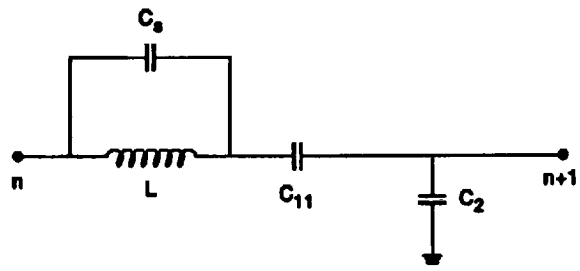

Figure 13 - Transmission line equivalent circuit model of the rippled-wall wave guide.

The TM_{0n} modes are solutions to the equation

$$\vec{\nabla} \times \vec{\nabla} \times \vec{H} - \frac{\omega^2}{c^2} \vec{H} = 0 \tag{28}$$

where $\vec{H} \cdot \hat{n} = 0$ at the boundary. Finding the dispersion relation for these modes is equivalent to finding the resonance frequencies of a section of the structure.

Using an established simulation technique [42], the resonant frequencies of a section of the structure, n periods in length and shorted at mirror symmetry planes, can be numerically or experimentally determined. These frequencies correspond to phase shifts per period from 0 to $(n-1)\pi/n$. The data is then fitted to a function resulting from their own equivalent circuit model description for the rippled-wall wave guide, similar to a model developed by Curnow for coupled-cavity traveling-wave tubes [43]. They find that they need only consider one period of the structure to obtain sufficient data to be used in the Curnow model [42].

The transmission line equivalent circuit model for the rippled-wall wave guide yields the dispersion relation

$$\omega^2 = \left\{ LC_s + \left[\frac{4 \sin^2\left(\frac{k\Delta}{2}\right)}{LC_{\perp}} + \frac{1}{LC_{\parallel}} \right]^{-1} \right\}^{-1} . \tag{29}$$

In this expression, $k\Delta$ is the phase shift per period, C_s represents the capacitance per period due to surface charge on the opposing walls, $C_{\perp}$ and $C_{\parallel}$ are the capacitances per period due to the electric fields perpendicular and parallel to the guide walls, respectively, and L is the inductance per period.

One period of the structure, with ends selected at minimum radius points, was used to find the resonances with 0, $\pi/2$, and π phase shifts per period when the boundary condition $\vec{H} \times \hat{n} = 0$ was applied at none, one, and both ends of the structure, respectively.

A computer program, SUPERFISH [44], for evaluation of RF cavities with cylindrical symmetry was used to calculate the resonant frequencies of a cylindrical wave guide with an average diameter of 1.9 cm., a ripple period of 1.0 cm., and a 20% ripple. The distribution of the electric field lines for the TM_{01} mode in the rippled-wall wave guide was generated for $k\Delta = 0$, $\pi/2$, and π using one period and $k\Delta = \pi/4$ and $3\pi/4$ using two periods.

The frequencies calculated corresponding to 0, $\pi/2$, and π phase shifts per period were 11.9, 13.9, and 17.3 GHz, respectively. These resonant frequencies, with the associated phase shifts, were used in the dispersion relation to solve for LC_s, $LC_{\perp}$, and $LC_{\parallel}$, thereby uniquely determining the entire dispersion relation.

The validity of the relation was checked by finding the resonant frequencies corresponding to $\pi/4$ and $3\pi/4$ phase shifts per period. Using the dispersion relation, these frequencies were found to be 12.4 and 16.0 GHz.

A two period structure with the boundary condition $\vec{H} \times \hat{n}=0$ at one end was required to obtain the $\pi/4$ and $3\pi/4$ phase shift per period resonant frequencies using SUPERFISH. The result was 12.5 and 15.9 GHz. The agreement was within 1%.

Since the SUPERFISH code can deal with the case of a spatially varying dielectric inside the wave guide, dispersion characteristics of rippled-wall wave guides employing plasmas to increase output power [45] can be found. This technique was deemed relatively easy to use. The accuracy of the results is governed by the complexity of the circuit model chosen.

Frequency response can be predicted for traveling-wave structures by using field analysis methods as in Pierce [18], Sensiper [21], and Vayornis et al [46]. These methods, however, can become highly complicated. An alternative approach is to analyze these structures using circuit models as in Bolljahn and Matthaei [47] and Weiss [48]. Using circuit analysis techniques with the aid of high speed computing, these passive models can yield the basic propagation effects and frequency response characteristics of the structure.

Dunham [49] has used a 2-coupled line physical circuit model with which coupled lines can be connected to form a helix or serpentine structure (Figure 14).

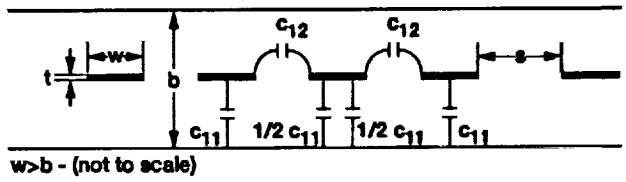

Figure 14 - Coupled-line model used for traveling-wave structures.

The dimension w is the width of the center conductor, t is the thickness of the center conductor, s is the distance between conductors, and b is the distance between ground planes.

The coupled lines serve as transmission-line elements and can have any impedance, length, or configuration, thus simulating any type of helix (Figure 15) or serpentine (Figure 16) structure.

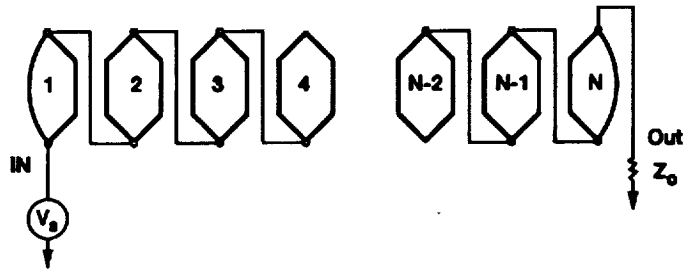

Figure 15 - Circuit model for the canonical helix structure.

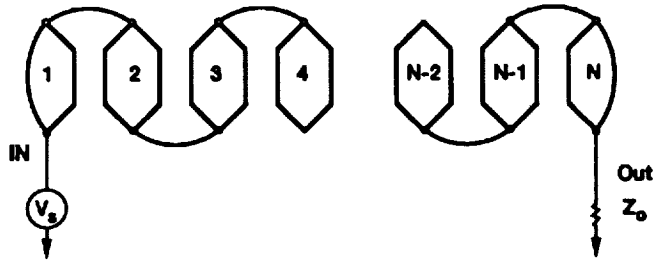

Figure 16 - Circuit model for the canonical serpentine structure.

The assumption of only nearest neighbor coupling in the model will adequately describe first order effects and structures in which higher order coupling has been suppressed due to shielding. The coupled stripline model is described by capacitances C_{11} and C_{12} and utilizes reduced coupler elements for forward and reverse coupling formed by splitting C_{11} into parallel $C_{11}/2$ capacitances. Since TEM propagation can occur, even- and odd-mode impedances, $Z_{\phi e}$ and $Z_{\phi o}$, can be defined.

For $w \geq b$, the total characteristic impedance Z and the mode impedances are given as

$$Z = \frac{1}{C_{11}^2 + 2C_{12}} \cdot \frac{1}{V} \cdot \begin{bmatrix} C_{11} + C_{12} & C_{12} \\ C_{12} & C_{11} + C_{12} \end{bmatrix}, \tag{30}$$

$$Z_{\phi e} = \frac{1}{VC_{11}}, \tag{31}$$

and

$$Z_{\phi o} = \frac{1}{V(C_{11} + 2C_{11})}. \tag{32}$$

This model accurately describes the common traveling-wave deflectors found in high frequency oscilloscopes. In particular, coupled line pairs with even-mode impedances of 50 and 100 ohms were considered to describe EG&G Energy Measurements, Inc. structures with $s = w$, and Tektronix structures with $s = w/2$. Only balanced structures were used for the former since the coupling ratio in single-ended structures does not depend on the value of b. The proper number of reduced coupled line elements was connected via ideal transmission lines in helix and serpentine arrangements with lengths of about 1450 ps and terminated in matching impedances.

The networks were then analyzed using Touchstone, a commercial microwave modeling program. An inverse FFT program was written by EG&G to operate on the S-parameter output of Touchstone to find the time response of the circuits. Only 100 output frequency points were available from Touchstone yielding 200 time points from the inverse FFT. The stimulus for the time response was created by integrating a Gaussian distribution for the rise portion of the signal and forcing even symmetry about the center of the time axis. The validity of the model was first checked by making the even- and odd-mode impedances of the structure equal for zero bar-to-bar coupling to simulate a dispersionless transmission line with no cutoff.

The physical lengths of the helix and serpentine structures analyzed were 1418 ps and 1463 ps, respectively. Both structures had a 100 Ω even-mode impedance and a 180° turn length at 4.1 GHz. It was found that the magnitude response was essentially constant for both structures, but the delay responses were markedly different; the helix delay response being flat while the serpentine delay response having over 600 ps of dispersion.

As a practical example, a single helix used as a vertical deflection structure for an EG&G KR-30 CRT traveling-wave oscilloscope was chosen for investigation. The S_{21} magnitude of the frequency response of the structure was measured using a network analyzer showing a main turn resonance at 7.2 GHz. An equivalent helix circuit model was developed based on the helix structure parameters for the KR-30 which included four capacitive supports and four coupler segments per turn (Figure 17).

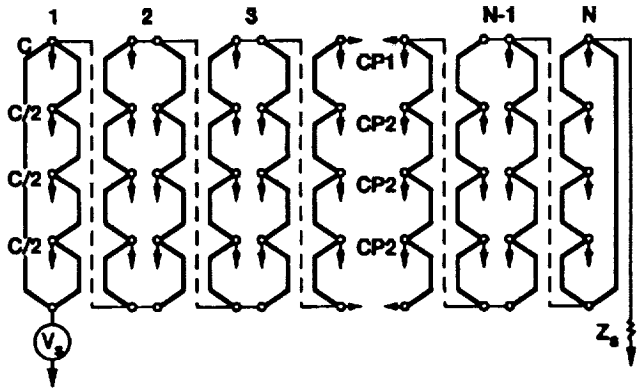

Figure 17 - Circuit for the exact modeling of the EG&G KR-30 structure.

The subsequent frequency response, transmission and delay, and time response of the model were generated for five cases:
1) Negligible coupling, loss, and capacitive loading,
2) Full coupling but with negligible loss and capacitance,
3) Periodic capacitive loading but with negligible coupling and loss,
4) Full coupling and capacitive loading but with negligible loss, and
5) Full coupling, capacitive loading, and mode loss included.
Each of these cases revealed different aspects of the model.

In case 1, the transmission and delay were found to be essentially constant with frequency and both having only a slight resonance at 7 GHz. This served as a fidelity test of the complete model.

Case 2 revealed the broad-band effects of coupling in the model while case 3 showed the narrow-band effects of periodic capacitive loading with a sharp resonance at 7.01 GHz. Slight positive "precursor" or noncausal pulse response and overshoot in the delay response were also evident.

Case 4 was essentially a linear combination of the effects from the previous two cases, however a negative precursor, characteristic of real helices, appeared in the delay response.

The main effect observed in case 5 was the reduced rise time of approximately 200 ps from previous cases. Broad-band resistive loss was also apparent from the transmission characteristics.

The effect of coupling in serpentine structures was also considered. Time response characteristics of a heavily coupled serpentine structure showed the effect of "ringing". In lightly coupled serpentine structures "precursor" was noticeable. There were important conclusions that followed from the modeling of broad-band traveling-wave structures.
1) The coupling ratio increases with structure impedance but signal transmission degrades.
2) In no loss situations, turn-to-turn coupling adversely affects serpentine structures but does not significantly affect helix structures. Shielding, however, can greatly improve the serpentine response.
3) Noncausal pulse response or "precursor" effects in the time response of a helix seems to be due to the combination of coupling and periodic capacitive perturbations while in a serpentine, phase distortion due to coupling is much greater than in a helix.
4) Skin effect loss and differential mode loss, both frequency dependent, are the major factors affecting the amplitude response in traveling-wave structures. Proper shielding allows the odd-mode current distribution and the mode loss to remain constant with frequency yielding higher bandwidths.

Efficiency enhancement

Efficiency of traveling-wave tubes can be enhanced in several ways. One such method involves tapering the periodicity of the slow-wave structure to adjust the phase velocity of the signal. A baseline ferruleless coupled-cavity TWT (Figure 18) of alternating webs and spacers [50] was used for the design of one such phase adjusted taper (PAT) by Wilson [51].

This tube consisted of three sections with the output section having 34 standard cavities, 9 cavities with the period shortened by 2.5%, and 6 cavities with the period 5.0% shorter. The RF saturation power with a 179 mA beam current and a 24.5 kV beam voltage was measured over a frequency range from 29.0 GHz to 30.0 GHz. These results compared well with the computer model at a beam voltage of 24.0 kV. The computer model beam voltages used for the design of the PAT are therefore 500 V lower than the experimental beam voltages.

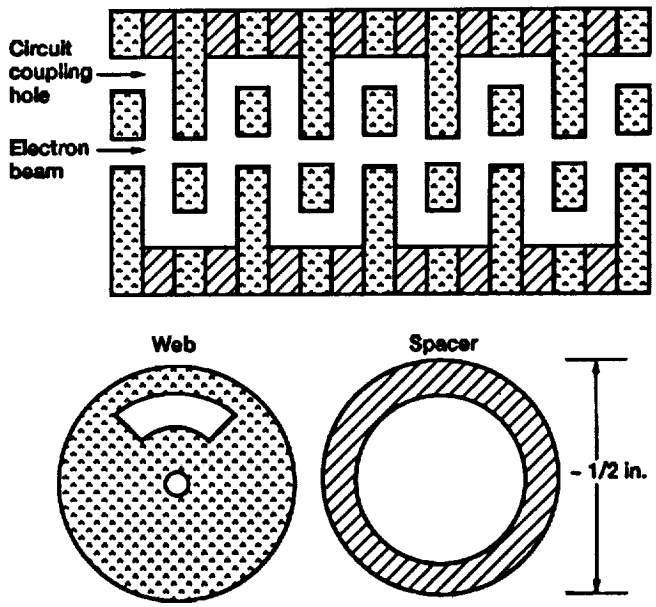

Figure 18 - Ferruleless coupled-cavity slow-wave structure with alternating copper webs and spacers.

The design procedure for the PAT consisted of several steps:

1) The first is the determination of the proper electron beam voltage to achieve the optimal RF interaction efficiency so that the phase of the electron beam with respect to the RF circuit wave at the start of the taper is between 0° and 45°.
2) Choose the proper cavity to start the taper while maintaining a high fundamental current.
3) The circuit phase velocity, v, and the electron beam velocity, u, are related to Pierce's velocity parameter, b, and Pierce's gain parameter, C, via the relationship $v = \frac{u}{1+bC}$. The gain parameter $C = \sqrt[3]{(KI)/(4V)}$, K is the interaction impedance, I is the beam current, and V is the beam voltage. A proper b must be determined so that the RF interaction efficiency remains high throughout the taper without unduly increasing the length and gain of the tube.

With the lengths of the cavities in the theoretical output section being the same, the fundamental beam current normalized to the initial total beam current and the electron bunch phase with respect to the RF circuit wave were calculated per cavity for beam voltages from 23.5 kV to 25.0 kV in 0.5 kV increments. A voltage of 23.5 kV was chosen for the design of the tube.

From the normalized fundamental beam current and electron bunch phase results, cavity 125 was chosen to start the taper. The RF interaction efficiency and and cavity periods for the taper were then calculated for $b = .00$, .05, .10, and .20. The value of $b = .10$ was chosen for the taper design. The computer generated PAT was 54 cavities long containing 45 different cavity lengths. For ease of fabrication, however, the final design was built utilizing 17 different cavity lengths to approximate the calculated PAT.

Final values for the RF interaction efficiency, normalized fundamental beam current, and phase of the electron bunch for the baseline TWT and the PAT TWT were computed as functions of the cavity number. The experimental values of RF output power and small signal gain were measured for the baseline TWT, operating at 24.5 kV and 179 mA, and the PAT TWT, operating at 24.0 kV and 184 mA. The PAT TWT showed marked improvement in power, gain, and efficiency over the baseline TWT. The calculated values compared very well to experimentally measured values.

Instabilities

Instabilities in coupled-cavity traveling-wave tubes (CCTWTs) can occur when there are high signal reflections due to mismatches at the output of the tube or if the circuit loss is not great enough. Also since the CCTWTs exhibit passbands and stopbands, oscillations due to high gain and high reflections at a band edge can occur, although less frequently, at the higher passbands [52].

Karp and Hunter [53] have addressed the issue of instabilities or oscillations in coupled-cavity tubes due to beam interaction with some of the higher order modes supported on the structure. They found that a relatively small number of CCTWTs exhibited these oscillations.

The most common cavities used in production tubes are the circular, square, and rectangular formats, along with some other variations, having a circular beam gap/tunnel with or without ferrules. The three coupling schemes that are used are either the 2 slots/in-line although used infrequently, the 1 slot/staggered, or the 2 slots/turn-staggered (Figure 19).

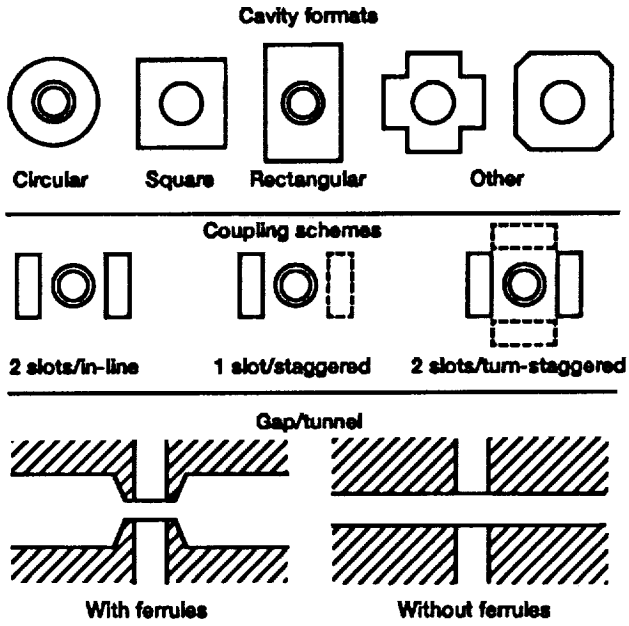

Figure 19 - Schematic of the coupled-cavity TWT circuit options.

Instabilities were found to occur regardless of the type of cavity format, gap/tunnel, magnetic focusing, or coupling scheme. All CCTWT structures can support higher order modes but the beam may or may not interact with them. Fundamental and second order mode symmetry conditions were considered for the three most common cavity formats, circular, square, and rectangular. The composite Brillouin diagrams of the fundamental and second order cavity and slot band modes for all three coupling schemes were determined.

From these considerations of the second order antisymmetric modes existing in a CCTWT, it was deemed plausible that if an electron beam could excite a mode of this type then the possibility of "trapping" RF energy in a section of the tube as a standing wave would be high. The section would, in effect, act as an "extended interaction" klystron (EIK) with regard to the second order mode. Certain resonances in the section, for a given beam velocity and conductance, may therefore, exhibit a negative beam-loading Q resulting in oscillation of the CCTWT. The CCTWTs studied seemed to have oscillations due to resonances in the second order cavity band.

Higher order mode oscillations were found to make themselves evident at frequencies near 1.5 times that of the fundamental cavity resonance. The signal gain probably would be less than suspected with the possible exception of "spikes" at certain frequencies. Four Varian CCTWTs of different construction and different operating parameters were found to exhibit higher order mode oscillation.

The gain of a TWT designed to operate in the fundamental mode is given by

$$G = -A + BCN \tag{33}$$

where $C = k'(I_0/V_0)^{1/3}$ depends on the cube root of the beam current value [18]. The condition for EIK oscillation, however, is directly proportional to the beam current and is satisfied by

$$kN \frac{I_0}{V_0} Q > 1. \tag{34}$$

The argument is that TWTs operating at high beam currents would be more likely to undergo higher order mode oscillation.

Consideration of beam conductance, section length, and effective circuit Q, when designing a CCTWT, are found to be important in suppressing the so called "trapped" waves responsible for higher order mode oscillations. The addition of circuit loss and geometrical modifications to change the beam filling factor can greatly reduce the possibility of EIK oscillation while only slightly affecting the gain and performance of the TWT.

Other considerations such as the gap transit angle and gap to gap phase shift were also considered important. Three-dimensional computer analysis and simulation of CCTWTs was stated to be the only viable means of dealing with this special instability. The instabilities arising from the electron beam interaction with higher order antisymmetric modes in a CCTWT can be predicted for a given set of parameters using several available computer codes.

Two such codes used by Friedlander, et al [54] for transient analysis of these interactions using a truncated periodic structure, are the Magnetic Insulation Code (MAGIC) and the Self-Optimized Sector (SOS) code. MAGIC [55] can simulate plasma physics problems and can solve electrodynamic problems in two dimensions using a self-consistent particle-in-cell (PIC) method. SOS [56] can solve similar problems in three dimensions.

The beam-loading Q of a lossless re-entrant klystron cavity was initially found from the relationship $Q = \pi f_0/\alpha$ [57] where f_0 is the cavity resonant frequency and α is the exponential signal decay rate. By exciting the dominant TM_{010} mode of the cavity with the introduction of an electron beam, so as not to excite signals above approximately 3.6 GHz, the time varying axial electric field component could be measured at the center of the interaction gap. From this measurement, α was determined.

The two lowest mode resonant frequencies were then determined using MAGIC and checked using the two-dimensional steady state electromagnetic code SUPERFISH [44]. The lowest mode resonant frequency f_0 was found to be 2.38 GHz using MAGIC compared to 2.386 GHz using SUPERFISH. Their resulting Q for this mode was approximately 40 which compared well with the value of 48 obtained conventionally [58].

A representative 80 cavity CCTWT with a typical beam current of 0.1 A was modeled with an eight ferruleless coupled-cavity lossless section of a circuit using a one slot staggered coupling arrangement having a 90° rotation between pairs (Figure 20).

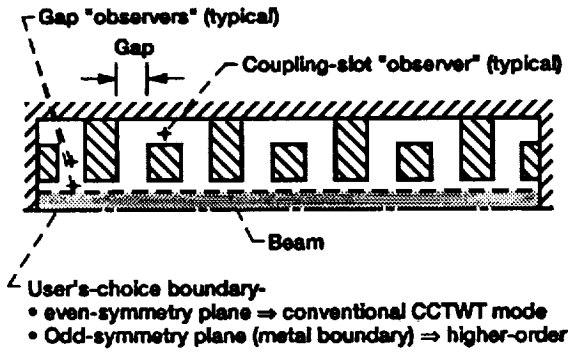

Figure 20 - Schematic of the eight-gap coupled-cavity TWT circuit model with locations of the field "observers" and the mode-selecting symmetry plane.

A beam current of 15 A was used for the model since the start oscillation Q is proportional to the product of the number of cavities and beam current to first order. Due to the increased beam perveance the average beam injection energy was raised to 22 keV. Symmetry conditions on the fields of the cavities were chosen to consider the dominant mode or the next higher antisymmetric mode. The computer code SOS was used to calculate the time history of the gap and slot fields. From the discrete Fourier transform, resonances in the lowest passband and higher order passbands were found. The computed frequency passband data compared very well with the measured frequency and phase data for resonances in the coupled-cavity circuit.

In order to analyze a particular resonance and reduce spurious responses using SOS, several techniques were incorporated.
1) Establishing a cutoff frequency for excited modes by using a finite turn-on time for the beam.
2) Neglecting the sharp turn-on transient in the field time history.
3) Eliminating the dc component of the time history to remove step pulse effects.
4) Finding the discrete Fourier transform of the modified time history.
5) Filtering the discrete Fourier transform to obtain the particular signal.
6) Finding the inverse discrete Fourier transform to obtain the "filtered" time response.

From the filtered time response, the growth rate of the signal was found for a particular higher order mode resonance. With proper scaling for an 80 cavity circuit with 0.1 A beam current, a start-oscillation Q of approximately 5000 was deduced. This was the first time a fully three-dimensional code has been used to calculate the stability threshold for an antisymmetric mode in a coupled-cavity circuit with a beam.

Millimeter-Wave Structures

There are a variety of millimeter-wave structures under consideration at the present time. A broad review on the status of recent research on various millimeter-wave tubes and devices is given by Feinstein and Felch [59]. Due to the reduced size of the slow-wave structure the fabrication and testing problems encountered can be considerable. Many times scaled versions of these structures are built and tested in order to assess the quality of similar structures at much higher frequencies.

REFERENCES

[1] K. Tsutaki, Y. Yuasa, and Y. Morizumi, "Numerical analysis and design for high-performance helix traveling-wave tubes," *IEEE Trans. Elec. Dev.*, vol. ED-32, no. 9, pp. 1842-1849, Sep., 1985.

[2] S. P. Otsuka, "Comments on 'Numerical analysis and design for high-performance helix traveling-wave tubes'," *IEEE Trans. Elec. Dev.*, vol. ED-33, no. 11, pp. 1928-1929, Nov., 1986.

[3] P. K. Jain, K. V. R. Murty, S. N. Joshi, and B. N. Basu, "Effect of the finite thickness of the helix wire on the characteristics of the helical slow-wave structure of a traveling-wave tube," *IEEE Trans. Elec. Dev.*, vol. ED-34, no. 5, pp. 1209-1213, May, 1987.

[4] B. N. Basu, R. K. Jha, A. K. Sinha, and L. Kishore, "Electromagnetic wave propagation through an azimuthally perturbed helix," *J. Appl. Phys.*, vol. 58, pp. 3625-3627, 1985.

[5] B. N. Basu and S. N. Joshi, "A heuristic formula for the dielectric loading factor of a helix supported by a dielectric circular rod," *Indian J. Appl. Phys.*, vol. 18, pp. 63-64, 1980.

[6] P. K. Jain and B. N. Basu, "The effect of conductivity losses on propagation through the helical slow-wave structure of a traveling-wave tube," *IEEE Trans. Elec. Dev.*, vol. ED-35, no. 4, pp. 549-558, Apr., 1988.

[7] J. E. Rowe, "Nonlinear Electron-Wave Interaction Phenomena," New York: Academic, ch. 3, 1965.

[8] J. H. Bryant and E. J. White, "Attenuation and power handling capability of helical radio-frequency lines," *IRE Trans. Microwave Theory Tech.*, vol. MTT-1, pp. 33-38, 1953.

[9] A. S. Gilmour, M. R. Gillette, and J. T. Chen, "Theoretical and experimental TWT helix loss determination," *IEEE Trans. Elec. Dev.*, vol. ED-26, pp. 1581-1588, 1979.

[10] P. K. Jain and B. N. Basu, "A theory of the attenuator-coated helical slow-wave structure of a traveling-wave tube," *IEEE Trans. Elec. Dev.*, vol. ED-35, no. 10, pp. 1750-1757, Oct., 1988.

[11] S. E. Webber, "Calculation of wave propagation on a helix in the attenuation region," *IRE Trans. Elec. Dev.*, vol. ED-1 pp. 35-39, Aug., 1954.

[12] J. J. Caldwell, "High power traveling-wave tube gain and saturation characteristics as a function of attenuator configuration and resistivity," *IRE Trans. Elec. Dev.*, vol. PGED-4, pp. 28-33, Dec., 1953.

[13] P. K. Jain and B. N. Basu, "The inhomogeneous loading effects of practical dielectric supports for the helical slow-wave structure of a TWT," *IEEE Trans. Elec. Dev.*, vol. ED-34, no. 12, pp. 2643-2648, Dec., 1987.

[14] J. L. Putz and M. J. Cascone, "Effective use of dispersion shaping in broad-band helix TWT circuits," *IEDM Tech. Dig.*, pp. 422-424, 1979.

[15] E. F. Belohoubek, "Helix support structure for ultra-wide-band traveling-wave tubes," *RCA Rev.*, vol. 26, pp. 106-117, 1965.

[16] S. Kapoor, R. S. Raju, R. K. Gupta, S. N. Joshi, and B. N. Basu, "Analysis of an inhomogeneously loaded helical slow-wave structure for broad-band TWT's," *IEEE Trans. Elec. Dev.*, vol. 36, no. 9, pp. 2000-2004, Sep., 1989.

[17] V. P. Singh, K. V. R. Murty, and B. N. Basu, "Interaction impedance from the equivalent circuit parameters of a dielectric-loaded helical slow-wave structure of a traveling-wave tube," *IEEE Trans. Elec. Dev.*, vol. ED-35, no. 4, pp. 563-566, Apr., 1988.

[18] J. R. Pierce, "Traveling-Wave Tubes," pp. 229-232, New York: Van Nostrand, 1950.

[19] G. Mishra, V. K. Tripathi, and V. K. Jain, "Effect of plasma and dielectric loading on the slow-wave properties of a traveling-wave tube," *IEEE Trans. Elec. Dev.*, vol. 37, no. 6, pp. 1561-1565, Jun., 1990.

[20] D. A. Watkins, "Topics in Electromagnetic Theory", ch. 2, John Wiley & Sons, Inc., New York, NY, 1958.

[21] S. Sensiper, "Electromagnetic wave propagation on helical structures," *Proc. IRE*, vol. 43, p. 149, 1955.

[22] H. S. Uhm and J. Y. Choe, "Electromagnetic wave propagation in a conducting waveguide loaded with a tape helix," *IEEE Trans. Microwave Theory Tech.*, vol. MTT-31, p. 704, 1983.

[23] W. N. Cain and R. W. Grow, "The effects of dielectric and metal loading on the dispersion characteristics for contrawound helix circuits used in high-power traveling-wave tubes," *IEEE Trans. Elec. Dev.*, vol. 37, no. 6, pp. 1566-1578, Jun., 1990.

[24] C. K. Birdsall and T. E. Everhart, "Modified contrawound helix circuits for high-power traveling-wave tubes," Hughes Aircraft Company, Tech. Memo. 400, 1955.

[25] S. F. Paik, "Design formula for helix dispersion shaping," *IEEE Trans. Elec. Dev.*, vol. ED-16, pp. 1010-1014, Dec., 1969.

[26] B. N. Basu, B. B. Pal, V. N. Singh, and N. C. Vaidya, "Optimum design of a potentially dispersion-free helical slow-wave circuit of a broadband TWT," *IEEE Trans. Microwave Theory Tech.*, vol. MTT-32, pp. 461-463, Apr., 1985.

[27] C. Y. Chen, "Characteristics of vane-loaded helix slow-wave structure," *NTG Fachberichte: Elektronenroehren*, no. 85, pp. 27-31, May, 1983.

[28] N. P. Kravchenko, L. N. Loshakov, and Y. N. Pchel'nikov, "Computation of dispersion characteristics of a spiral placed in a screen with longitudinal ribs," *Radio Eng. Electron. Phys.*, vol. 21, pt. 1, pp. 33-39, Apr., 1976.

[29] A. W. Scott, "Dual-mode traveling-wave tube status report," Varian Assoc., Jun., 1973.

[30] P. Galuppi and C. Lamesa, "A new technique for ultra-broadband high power TWTs," *Proc. Military Microwave Conf.*, pp. 501-505, Oct., 1980.

[31] P. Galuppi and M. D. Salvatore, "Evaluation of three techniques of controlling phase velocity dispersion in helix TWT," *Proc. Int. Conf. Microwave Tubes in Systems: Problems and Prospects*, pp. 59-62, Oct., 1984.

[32] L. Kumar, R. S. Raju, S. N. Joshi, and B. N. Basu, "Modeling of a vane-loaded helical slow-wave structure for broad-band traveling-wave tubes," *IEEE Trans. Elec. Dev.*, vol. 36, no. 9, pp. 1991-1999, Sep., 1989.

[33] N. P. Kravchenko, L. N. Loshakov, and Yu. N. Pchel'nikov, "Computation of dispersion characteristics of a spiral placed in a screen with longitudinal ribs," *Radio Eng. Electron. Phys.*, vol. 21, pt. 1, pp. 33-39, Apr., 1976.

[34] T. Onodera and W. Raub, "Phase velocity dispersion of a generalized metal-segment-loaded helix as used in broad-band traveling-wave tubes," *IEEE Trans. Elec. Dev.*, vol. ED-35, no. 4, pp. 533-538, Apr., 1988.

[35] J. R. Legarra, "Measurement of microwave characteristics of helix traveling-wave circuits," *IEDM Tech. Dig.*, pp. 408-411, 1979.

[36] T. Onodera, "An analysis of the π-mode stopband caused by asymmetries of a metal-segment-loaded helix as used in broad-band traveling-wave tubes," *IEEE Trans. Elec. Dev.*, vol. ED-35, no. 10, pp. 1758-1759, Oct., 1988.

[37] E. L. Lien, "Stopbands produced by asymmetrical support rod system in helix structures," *IEDM Tech. Dig.*, pp. 412-415, 1979.

[38] T. Onodera, "Method for calculating the small-signal gain of a broad-band TWT with finite beam thickness," *IEEE Trans. Elec. Dev.*, vol. 37, no. 6, Jun., 1990.

[39] K. Ura and M. Terada, "Circuit parameters for thick beam in traveling-wave tubes theory," *J. Inst. Electron. Commun. Eng. Japan*, vol. 45, p. 1563, 1962 (in Japanese).

[40] K. Ura and M. Terada, "Circuit parameters for general slow-wave circuits and thick electron beams in traveling-wave tube theory," *Technol. Rep. Osaka Univ.*, vol. 12, no. 517, p. 297, 1962.

[41] F. D. Kantrowitz and E. A. Adler, "Calculation of TM_{0n} mode dispersion relations in rippled-wall waveguides," *IEEE Trans. Elec. Dev.*, vol. 37, no. 12, pp. 2619-2621, Dec., 1990.

[42] F. D. Kantrowitz and I. Tammaru, "Three-dimensional simulations of frequency-phase measurements of arbitrary coupled-cavity RF circuits," *IEEE Trans. Elec. Dev.*, vol. 35, no. 11, pp. 2018-2026, Nov., 1988.

[43] H. J. Curnow, "A general equivalent circuit for coupled-cavity slow-wave structures," *IEEE Trans. Microwave Theory Tech.*, vol. MTT-13, no. 5, pp. 671-675, Sep., 1965.

[44] K. Halbach and R. F. Holsinger, "SUPERFISH – A computer program for evaluation of RF cavities with cylindrical symmetry," *Part. Accel.*, vol. 1, 213-222, 1976.

[45] Y. Carmel, K. Minami, R. A. Kehs, W. W. Destler, V. L. Granatstein, D. Abe, and W. L. Lou, "Demonstration of efficiency enhancement in a high-power backward-wave oscillator by plasma injection," *Phys. Rev. Lett.*, vol. 62, no. 20, pp. 2389-2392, May, 1989.

[46] Z. A. Vaynoris, K. Matseyka, and S. Shtaras, "Analysis of two-spiral deflection systems," *Radio Eng. Electron. Phys.*, vol. 15, no. 6, p. 1125.

[47] J. Bolljahn and G. Matthaei, "A study of the phase and filter properties of arrays of parallel conductors between ground planes," *IRE Proc.*, vol. 50, p. 299, 1962.

[48] J. Weiss, "Dispersion and field analysis of a microstrip meander-line slow-wave structure," *IEEE Trans. Microwave Theory Tech.*, vol. MTT-22, p. 1194, 1974.

[49] M. E. Dunham, "Modern circuit models for traveling-wave structures with nearest neighbor coupling," *IEEE Trans. Elec. Dev.*, vol. 37, pp. 862-869, 1990.

[50] "Study of methods for the reduction of distortion in high power TWTs" contract number NAS3-24899.

[51] J. Wilson, "A high efficiency ferruleless coupled-cavity traveling-wave tube with phase adjusted taper," *IEEE Trans. Elec. Dev.*, vol. 37, no. 12, pp. 2638-2643, Dec., 1990.

[52] J. A. Ruetz, "Resonant circuit oscillations in traveling-wave tubes," *Proc. 4th Int. Congr. on Microwave Tubes*, Scheveningen: Centrex Publ. Co., p. 94, Sep., 1962.

[53] A. Karp and G. T. Hunter, "Higher order modes and instabilities in coupled-cavity TWTs," *IEEE Trans. Elec. Dev.*, vol. ED-33, no. 11, pp. 1890-1895, Nov., 1986.

[54] F. Freidlander, A. Karp, B. D. Gaiser, J. S. Gaiser, and B. Goplen, "Transient analysis of beam interaction with the antisymmetric mode in a truncated periodic structure using the three-dimensional computer code 'SOS'," *IEEE Trans. Elec. Dev.*, vol. ED-33, no. 11, pp. 1896-1901, Nov., 1986.

[55] B. Goplen, R. E. Clark, J. McDonald, and W. M. Bollen, "User's Manual for MAGIC/Version September 1983," Mission Research Corp. Rep. MRC/WDC-R-068, Sep., 1983.

[56] B. Goplen, R. J. Barker, R. E. Clark, and J. McDonald, "User's Manual for SOS/Version September 1983," Mission Research Corp. Rep. MRC/WDC-R-065, Sep., 1983.

[57] R. N. Ghose, "Microwave Circuit Theory and Analysis," p. 182, McGraw-Hill Book Company, New York, NY, 1963.

[58] G. Branch, Jr., "Electron beam coupling in interaction gaps of cylindrical symmetry," *IRE Trans. Elec. Dev.*, vol. ED-18, pp. 193-207, May, 1961.

[59] J. Feinstein and K. Felch, "Status review of research on millimeter-wave tubes," *IEEE Trans. Elec. Dev.*, vol. ED-34, no. 2, Feb., 1987.

REPORT DOCUMENTATION PAGE

Form Approved
OMB No. 0704-0188

1. AGENCY USE ONLY (*Leave blank*)	2. REPORT DATE	3. REPORT TYPE AND DATES COVERED
	June 1994	Technical Memorandum

4. TITLE AND SUBTITLE

Review of Slow-Wave Structures

5. FUNDING NUMBERS

WU-235-01-1C

6. AUTHOR(S)

Thomas M. Wallett and A. Haq Qureshi

7. PERFORMING ORGANIZATION NAME(S) AND ADDRESS(ES)

National Aeronautics and Space Administration
Lewis Research Center
Cleveland, Ohio 44135-3191

8. PERFORMING ORGANIZATION REPORT NUMBER

E-8943

9. SPONSORING/MONITORING AGENCY NAME(S) AND ADDRESS(ES)

National Aeronautics and Space Administration
Washington, D.C. 20546-0001

10. SPONSORING/MONITORING AGENCY REPORT NUMBER

NASA TM-106639

11. SUPPLEMENTARY NOTES

Thomas M. Wallett, NASA Lewis Research Center, and A. Haq Qureshi, NASA Resident Research Associate at Lewis Research Center. Responsible person, Thomas M. Wallett, organization code 5620, (216) 433-3673.

12a. DISTRIBUTION/AVAILABILITY STATEMENT

Unclassified - Unlimited
Subject Category 33

12b. DISTRIBUTION CODE

13. ABSTRACT (*Maximum 200 words*)

The majority of recent theoretical and experimental reports published in the literature dealing with helical slow-wave structures focus on the dispersion characteristics and their effects due to the finite helix wire thickness and attenuation, dielectric loading, metal loading, and the introduction of plasma. In many papers, an effective dielectric constant is used to take into account helix wire dimensions and conductivity losses, while, the propagation constant of the signal and the interaction impedance of the structure are found to depend on the surface resistivity of the helix. Also, various dielectric supporting rods are simulated by one or several uniform cylinders having an effective dielectric constant, while metal vane loading and plasma effects are incorporated in the effective dielectric constant. The papers dealing with coupled-cavities and folded or loaded wave guides describe equivalent circuit models, efficiency enhancement, and the prediction of instabilities for these structures. Equivalent circuit models of various structures are found using computer software programs SUPERFISH and TOUCHSTONE. Efficiency enhancement in tubes is achieved through dynamic velocity and phase adjusted tapers using computer techniques. The stability threshold of unwanted antisymmetric and higher order modes is predicted using SOS and MAGIC codes and the dependence of higher order modes on beam conductance, section length, and effective Q of a cavity is shown.

14. SUBJECT TERMS	15. NUMBER OF PAGES
Helix; Coupled-cavity; Slow-wave	30
	16. PRICE CODE: A03

17. SECURITY CLASSIFICATION OF REPORT	18. SECURITY CLASSIFICATION OF THIS PAGE	19. SECURITY CLASSIFICATION OF ABSTRACT	20. LIMITATION OF ABSTRACT
Unclassified	Unclassified	Unclassified	